Compact Transverse Electric Silicon-on-Insulator Mode Converter for Mode-Division Multiplexer

Mohamed H. Sharaf, Mohamed B. El-Mashade, and Ahmed A. Emran

Abstract—On-chip optical-interconnect technology emerges as an attractive approach due to its ultra-large bandwidth and ultra-low power consumption. Silicon-on-insulator (SOI) wire waveguides, on the other hand, have been identified to potentially replace copper wires for intra-chip communication. To take advantage of the wide bandwidth of SOI waveguides, wavelength-division multiplexing (WDM) has been implemented. However, WDM have inherent drawbacks. Mode-division multiplexing (MDM) is a viable alternative to WDM in MIMO photonic circuits on SOI as it requires only one carrier wavelength to operate. In this vein, mode converters are key components in on-chip MDM systems. The goal of this paper is to introduce a transverse electric mode converter. The suggested device can convert fundamental transverse electric modes to first-order transverse electric ones and vice versa. It is based on small material perturbation which introduces gradual coupling between different modes. This device is very simple and highly compact; the size of which is 3 μm^2. Mathematical expressions for both the insertion loss and crosstalk are derived and optimized for best performance. In addition, three-dimensional finite-difference time-domain (3D-FDTD) simulations are performed in order to verify the mathematical model of the device. Our numerical results reveal that the proposed device has an insertion loss of 1.2 dB and a crosstalk of 10.1 dB. The device's insertion loss can be decreased to 0.95 dB by adding tapers to its material perturbation.

Keywords—integrated optics; silicon-on-insulator waveguide; WDM & MDM systems; perturbation theory; integrated optical devices; hybrid modes; guided waves

I. INTRODUCTION

A STEADILY increasing bandwidth is the basic demand of recent optical communication systems. However, replying such demand could not be achieved simply by scaling the electro-optical bandwidth of modulators and detectors. Therefore, multiplexing techniques are needed for the aggregate bandwidth of a link to be increased. The principal of these techniques is the orthogonality among different physical properties of light, such as polarization or wavelength. In this regard, wavelength division multiplexing (WDM) and polarization division multiplexing (PDM) are widely used nowadays. While the first makes use of different wavelengths to transmit different data, the later exploit the polarization state of light (usually TE and TM) to multiplex data. However, in the order of several hundreds of Tbps, future optical interconnects are expected to deliver bandwidths. In that

framework, WDM scenarios will soon attain their limit and they haven't the capability to follow that request of bandwidth anymore [1] A new orthogonality level dependent on the spatial distribution of optical field within a waveguide has been recently proposed. This model uses the different optical modes of a waveguide to multiplex data and is called mode division multiplexing (MDM). As a medium of communication, current MDM systems make use of either optical fiber or free-space optics [2]. In planar integrated technology, however, MDM systems are not developed. Meanwhile, it will be desirable to develop integrated photonics transceivers with mode diversity (i.e. MDM). In order to fulfill such functionalities, two basic building blocks are required; the mode multiplexer (MM) and the mode converter (MC). In other words, to efficiently implement MDM systems, several building blocks have to be developed. These blocks include mode converters and mode filters, which are currently studied to have high-performance and compact sizes.

From the implementation point of view, an on-chip MDM switch, based on single-mode ring resonators, has been established in [3]. Also, a higher-order mode-pass filter, based on one-dimensional periodic structures, has been demonstrated in [4]. Additionally, a switchable dual-mode exchanger, which consists of two symmetric Y-junctions and a phase shifter, has been studied in [5]. The aim of the resulting system is to be tunable while sacrificing the compactness of the device. Its size is 60 μm x 3 μm. It is developed for using in tunable mode filter [6]. Another higher order mode-pass filter, based on dual-mode conversion, has been investigated for optical fiber [7]. Mode converters based on binary phase plates is introduced in [8] for optical fiber. The same idea of these converters is developed for silicon-on-insulator (SOI) with an insertion loss of 1.5 dB and a device size of 5 μm x 1 μm [9]. In [10], the authors used a Bragg grating with a resonator cavity. The device targeted a frequency selective response, and thus it is bulky with a size of 210 μm x 1.02 μm and an insertion loss of 2.1 dB. Our proposed device has the most compact size, 3 μm x 1.05 μm, a modest insertion loss (1.2 dB) and a crosstalk of 10.1 dB. An improvement is made for its insertion loss to become 0.95 dB.

In this paper, we propose a simple mode converter based on a small material perturbation. The idea of material perturbation is introduced in [11] and is applied for a polarization rotator which is used in single mode systems with a device length of 210 μm. The same idea is applied here for a transverse electric mode converter which is used in multimode systems. The

Mohamed H. Sharaf, Mohamed B. El-Mashade, and Ahmed A. Emran are with Electrical Engineering Department, Faculty of Engineering, Al-Azhar University, Cairo, Egypt (e-mail: {m.sharaf, mohamed.b.elmashade, ahmed.emran}@azhar.edu.eg).

device introduces gradual coupling between different modes. To elaborate on the idea, we present a mode converter between the fundamental hybrid mode like (HE_{11}) and the first-order hybrid mode like (HE_{21}). The size of the suggested device is $3\ \mu m^2$ which is highly compact. Its bandwidth is very wide around a wavelength of $1550\ nm$. The insertion loss is $1.2\ dB$ with a crosstalk of $10.1\ dB$ at its output port. An improvement is introduced in the form of two tapers in the propagation direction. The modified version has an insertion loss of $0.95\ dB$ at the expense of $9.2\ dB$ crosstalk which is slightly higher.

To evaluate the device performance, we develop a mathematical model for the proposed mode converter based on perturbed coupled mode theory [12]. The impacts of the phase mismatch between the two modes, self-mode coupling, and coupling to other parasitic modes are studied. Using the mathematical expressions, we optimize the dimensions of the structure. In addition, three-dimensional finite-difference time-domain simulations (3D-FDTD) are achieved. The simulation results are shown to be in good agreement with the mathematical model. In addition, it is illustrated that the device has good insertion loss and low crosstalk, and high bandwidth along with its simplicity. The rest of this paper is organized as follows. The structure of the proposed mode converter is outlined in section II. The mathematical model representation is discussed in section III. Section IV displays the 3D-FDTD simulations for different values of the device parameters. Finally, section V concludes the paper.

II. PROPOSED MODE CONVERTER STRUCTURE

Fig. 1. Structure of HE_{11} to HE_{21} mode converter (top view)

Figure 1 presents the structure of the HE_{11} to HE_{21} mode converter. It consists of a silicon strip waveguide with width w and height h. The cladding and substrate are both silicon dioxide SiO_2. A small material perturbation in the form of a vertical rectangle of silicon dioxide is introduced, with width g and distance d between the center of the perturbation and center of the waveguide. Using the perturbation method, the effective index difference between the waveguide before and after introducing the perturbation can be modeled as:

$$\Delta n(x,y) = \begin{cases} 0; & \text{if } -w/2 < x < d - g/2, 0 \le y \le h, \\ n_{\text{SiO}_2} - n_{\text{Si}}; & \text{if } d - g/2 \le x \le d + g/2, 0 \le y \le h, \\ 0; & \text{if } d + g/2 < x < w/2, 0 \le y \le h, \end{cases} \tag{1}$$

where $n_{\text{SiO}_2} = n_2$ is the refractive index of silicon dioxide and $n_{\text{Si}} = n_1$ is the refractive index of silicon.

A. Theoretical Analysis

In this section, we aim at developing mathematical equations relating the input and output HE modes. The derivation is based on perturbated coupled mode theory. The perturbed device is a strip waveguide. We do not include the effect of the return loss as the perturbation is small relative to the strip dimensions. The crosstalk is analyzed through studying the coupling to undesired modes in the output.

1) Electric Field Expressions: For any transverse electric-like HE_{pq} mode, $p, q \in \{1, 2, \dots\}$, in a strip wave guide, the electric field can be expressed as [13]:

$$E(x,y,z) = A(z)e^{j(\omega t - \beta z)}\Psi(x,y), \tag{2}$$

where $A(z)$ is the complex amplitude of the field along the propagation direction z, ω is the angular frequency of the wave, β is the phase constant and $\Psi(x,y)$ is the field profile function in the transverse plane. Since the wave guide has $w > h$, and h is relatively small, then the HE_{pq} modes will

be restricted HE_{p1} modes. Using the effective-index method (EIM), $\Psi(x,y)$ can be expressed as:

$$\Psi(x,y) = G_l(y)F_m(x), \tag{3}$$

where $m = p - 1$ and $l = q - 1$. Here,

$$G_l(y) = \begin{cases} B_l \cos(\phi)e^{\gamma_l y}; & \text{if } y < 0, \\ B_l \cos(\rho y - \phi); & \text{if } 0 \le y \le h, \\ B_l \cos(\rho h - \phi)e^{-\gamma_l(y-h)}; & \text{if } h < y, \end{cases} \tag{4}$$

where $\gamma_l = \frac{2\pi}{\lambda_o}\sqrt{n_{\text{effg}_l}^2 - n_2^2}$, n_{effg_l} is the effective index of a slab waveguide of height h in y direction, λ_o is the wavelength of operation, $\rho = \frac{2\pi}{\lambda_o}\sqrt{n_1^2 - n_{\text{effg}_l}^2}$, and $\phi = \rho h/2 + l\pi/2$. B_l is a constant that can be expressed as [14]:

$$B_l = \sqrt{\frac{2}{h + \frac{2}{\gamma_l}}}. \tag{5}$$

Since $q = 1$ then $l = 0$, $\phi = \rho h/2$ and $B_l = B_0$ for all HE_{p1} modes. The x component for HE_{p1} mode $p = m + 1$ can be expressed as:

$$F_m(x) = \begin{cases} C_m \frac{N_{\text{wg}_m}\eta_o}{n_2^2}\cos(\frac{-\alpha_m w}{2} - \frac{m\pi}{2})e^{\sigma_m(x+w/2)}; & \text{if } x < -w/2, \\ C_m \frac{N_{\text{wg}_m}\eta_o}{n_{\text{effg}_l}^2}\cos(\alpha_m x - \frac{m\pi}{2}); & \text{if } |x| \le w/2, \\ C_m \frac{N_{\text{wg}_m}\eta_o}{n_2^2}\cos(\frac{\alpha_m w}{2} - \frac{m\pi}{2})e^{\sigma_m(x-w/2)}; & \text{if } w/2 < x, \end{cases} \tag{6}$$

C_m^2 can be expressed as [14]:

$$C_m^2 = \frac{4n_{\text{effg}_l}}{N_{\text{wg}_m}\left(w + \frac{2}{\sigma_m}\left(\frac{n_{\text{effg}_l}}{n_2}\right)^2 \frac{1+\left(\frac{\sigma_m}{\alpha_m}\right)^2}{1+\left[\left(\frac{n_{\text{effg}_l}}{n_2}\right)^2 \cdot \left(\frac{\sigma_m}{\alpha_m}\right)\right]^2}\right)}. \tag{7}$$

where $\sigma_m = \frac{2\pi}{\lambda_o}\sqrt{N_{\text{wg}_m}^2 - n_2^2}$, $N_{\text{wg}_m}^2$ is the effective index of the strip waveguide for mode $\text{HE}_{(m+1)1}$, $\alpha_m = \frac{2\pi}{\lambda_o}\sqrt{n_{\text{effg}_l}^2 - N_{\text{wg}_m}^2}$.

2) Coupled Mode Equations: Starting from the coupled mode general equation:

$$j2\sum_m \beta_m \Psi_m(x,y)\frac{dA_m}{dz}e^{-j\beta_m z} = k_0^2 \Delta n^2(x,y)\sum_m A_m(z)\Psi_m(x,y)e^{-j\beta_m z}, \tag{8}$$

where $k_0 = \frac{2\pi}{\lambda_0}$ is the wave number in free space. Multiplying (8) by Ψ_n^* then integrating over x and y, and simplifying, we get:

$$e^{-j\beta_n z}\frac{dA_n}{dz} = -j\frac{\omega\epsilon_0}{4\eta_0}\frac{n_{\text{effg}}^3}{N_{\text{wg}_n}^2}\sum_m A_m(z)e^{-j\beta_m z}\iint \Psi_n^*(x,y)\Delta n^2(x,y)\Psi_m(x,y)dxdy, \tag{9}$$

where ϵ_0 is the electric permittivity in free space, $\eta_0 = \sqrt{\mu_o/\epsilon_0}$ is the wave impedance in free space, μ_o is the magnetic permeability in free space. Defining:

$$\kappa_{nm} = \frac{\omega\epsilon_0}{4\eta_0}\frac{n_{\text{eff}_g}^3}{N_{\text{wg}_n}^2}\iint \Psi_n^*(x,y)\Delta n^2(x,y)\Psi_m(x,y)dxdy. \tag{10}$$

(9) reduces to:

$$e^{-j\beta_n z}\frac{dA_n}{dz} = -j\sum_m \kappa_{nm}A_m(z)e^{-j\beta_m z}. \tag{11}$$

Assuming input mode l, output mode m and interference mode n, the coupled mode equations can be simplified to:

$$\frac{d\boldsymbol{X}}{dz} = \mathbf{A}\boldsymbol{X}, \tag{12}$$

where

$$\boldsymbol{X}(z) = \begin{bmatrix} x_l \\ x_m \\ x_n \end{bmatrix} = \begin{bmatrix} A_l e^{-j\beta_l z} \\ A_m e^{-j\beta_m z} \\ A_n e^{-j\beta_n z} \end{bmatrix} \tag{13}$$

$$\mathbf{A} = \begin{bmatrix} -j(\beta_l + \kappa_{ll}) & -j\kappa_{lm} & -j\kappa_{ln} \\ -j\kappa_{ml} & -j(\beta_m + \kappa_{mm}) & -j\kappa_{mn} \\ -j\kappa_{nl} & -j\kappa_{nm} & -j(\beta_n + \kappa_{nn}) \end{bmatrix}. \tag{14}$$

3) Evaluation of Coupling Coefficients: In this subsection, we evaluate the inter-modal coupling coefficients κ_{nm} between modes $\text{HE}_{(n+1)1}$ and $\text{HE}_{(m+1)1}$. In addition, we evaluate the self-coupling κ_{mm} of mode $\text{HE}_{(m+1)1}$. Defining $Q_n = \frac{\omega\epsilon_0}{4\eta_0}\frac{n_{\text{effg}}^3}{N_{\text{wg}_n}^2}$ and $R_n = \frac{N_{\text{wg}_n}\eta_0}{n_{\text{effg}_l}^2}$, it is easy to check that:

$$\kappa_{mm} = \frac{Q_m B_0^2 C_m^2 R_m^2 (n_{SiO2}^2 - n_{Si}^2)}{4}\left[\left(g - \frac{\sin[2(\alpha_m(d-g/2)-0.5m\pi)]}{2\alpha_m} + \frac{\sin[2(\alpha_m(d+g/2)-0.5m\pi)]}{2\alpha_m}\right) \times \left[h + \frac{\sin[2(\rho h - \phi)]}{2\rho} - \frac{\sin(-2\phi)}{2\rho}\right]\right] \tag{15}$$

and

$$\kappa_{nm} = \frac{Q_n B_0^2 C_n R_n C_m R_m (n_{SiO2}^2 - n_{Si}^2)}{4}\left[\left(\frac{\sin[(\alpha_n + \alpha_m)(d+g/2)-0.5(m+n)\pi]}{(\alpha_n + \alpha_m)} - \frac{\sin[(\alpha_n + \alpha_m)(d-g/2)-0.5(m+n)\pi]}{(\alpha_n + \alpha_m)}\right) + \left(\frac{\sin[(\alpha_n - \alpha_m)(d+g/2)-0.5(n-m)\pi]}{(\alpha_n - \alpha_m)} - \frac{\sin[(\alpha_n - \alpha_m)(d-g/2)-0.5(n-m)\pi]}{(\alpha_n - \alpha_m)}\right)\right] \times \left[h + \frac{\sin[2(\rho h - \phi)]}{2\rho} - \frac{\sin(-2\phi)}{2\rho}\right], \tag{16}$$

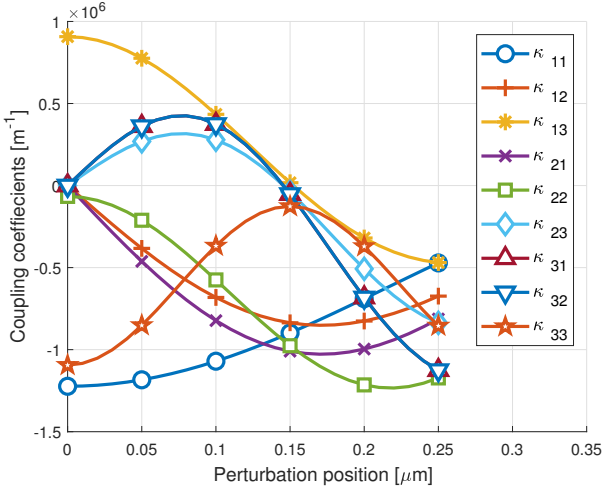where B_0^2, C_n, and C_m are determined from (6) and (7).

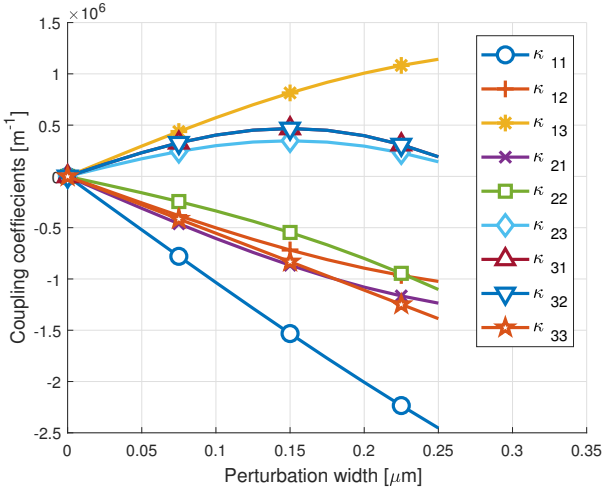Fig. 2. Coupling coefficients versus perturbation position

Fig. 3. Coupling coefficients versus perturbation width

From (10), it is noticed that the coupling coefficient is affected by the intersection between the perturbation profile $\Delta n(x, y)$ and the electric field profiles $\Psi(x, y)$. Figures 2 and 3 show the variation of coupling coefficients versus perturbation dimensions. In Fig. 3, it is observed that the coupling coefficients start at zero when the perturbation width is zero.

III. 3D FDTD SIMULATIONS AND NUMERICAL RESULTS

In this section, we present our simulation results for proposed device. The simulation is performed using three-dimensional finite-difference time-domain method (3D FDTD). The device is simulated using a strip waveguide width of 1.05 μm and height of 0.22 μm . The perturbation width is 100 nm and its center is translated 80 nm from the waveguide center. The length of the perturbation along the propagation direction is 2.7 μm to get the maximum coupling between the two desired modes. It is noted that the length of the
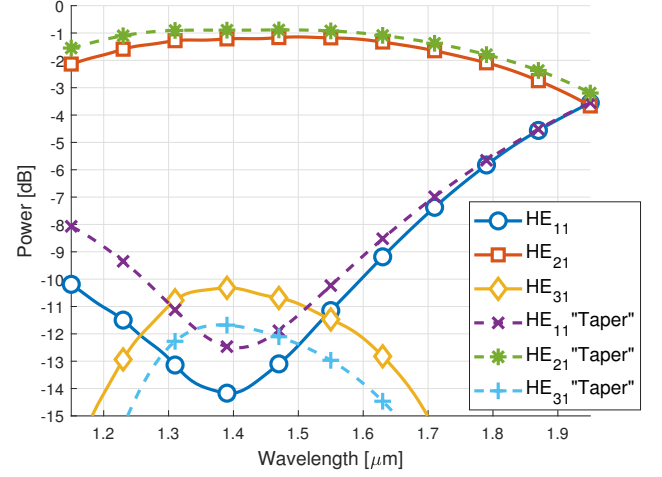

Fig. 4. Output power in HE_{11}, HE_{21} and HE_{31} modes vs. Wavelength

perturbation that is extracted from simulation is consistent with that estimated by the mathematical model.

A. Power vs. Wavelength

Figure 4 depicts the modes powers at the output for the perturbation structure. It is observed that at a wavelength of 1550 nm and when the perturbation is rectangular, the desired mode HE_{21} has an insertion loss of 1.2 dB with crosstalks of 10.1 dB and 10.2 dB to both HE_{11} and HE_{31} modes, respectively.

B. Power vs. Perturbation Length

Fig. 5 shows the output power distributed on HE_{21} and HE_{11} modes with respect to the length of the perturbation along the propagation direction L. It is shown in Fig. 5 that the output power of the desired mode HE_{21} exhibits its maximum when L is equal to 3 μm. The simulation is in good agreement with the mathematics. Due to the approximation in effective index method and perturbed coupled mode theory, the actual device length obtained from the 3D FDTD simulations was 2.7 μm.

IV. RESULTS DISCUSSION

Observing the mathematical analysis, the goal of the system is to increase the coupling between the input and output modes. (16) shows that the perturbation parameters (width, center position, and material) in addition to the waveguide width affect the amount of coupling between different modes. Specifically, from (16), if the width increases then the inter-modal and self-modal coupling will increase as long as the field profiles are coupled constructively (both positive or both negative in the transverse plane). Increasing the width will eventually increase the coupling from interference modes and introduce constructive coupling between field profiles thus degrading the performance. In addition, the perturbation center position depicts the region in which the field profiles of the modes interact. Choosing a region with high intersection of
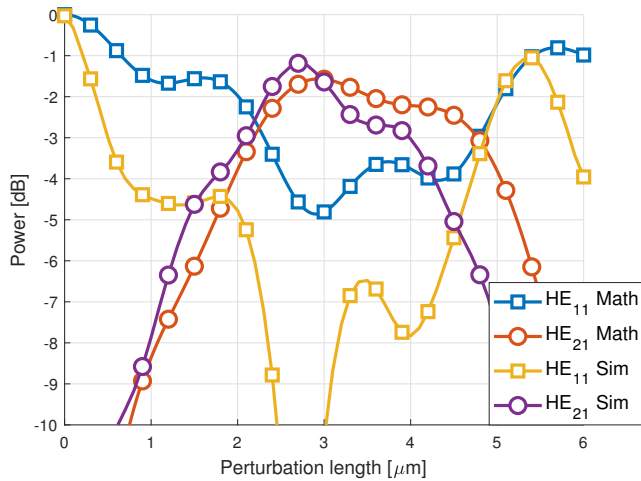
Fig. 5.   Output power for HE_{11} and HE_{21} modes vs. perturbation length

Fig. 7. E_y field profile for tapered perturbation structure

field profiles in the transverse plane will increase the performance, but also will increase the interference between the input and undesired interference modes. Regarding the material, increasing the difference in the effective index between the waveguide material and the perturbation material will improve the coupling at the expense of more return loss. Decreasing the perturbation area in the transverse plane decreases the return loss. Although, the backward traveling mode is neglected in our mathematical analysis, the 3D-FDTD simulation estimated a return loss of 0.3 dB for mentioned device dimensions. The width of the waveguide affects input-output coupling. From the mode chart figure in [14], when the width increases, the difference in the effective index decreases thus the phase mismatch decreases. On the other hand, increasing the width will permit other undesired higher order modes to propagate thus increases the crosstalk.
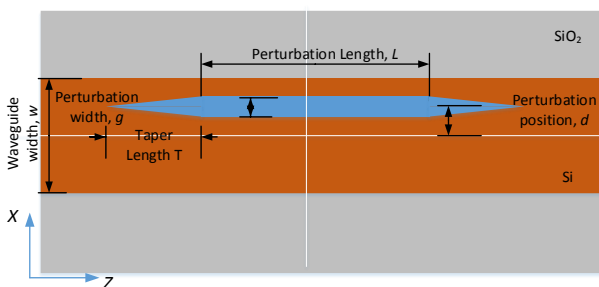
A. Insertion Loss Improvement

Fig. 6.   Structure of HE_{11} to HE_{21} mode converter with tapers (top view)

An improvement in the form of two tapers at the start and end of the perturbation along the propagation direction is shown in 6. The tapers have a base of 100 nm and height of 300 nm. The modes powers at the output for the improved tapered structure is depicted in Fig. 4 as well. It is observed that the insertion loss is slightly decreased to 0.95 dB but
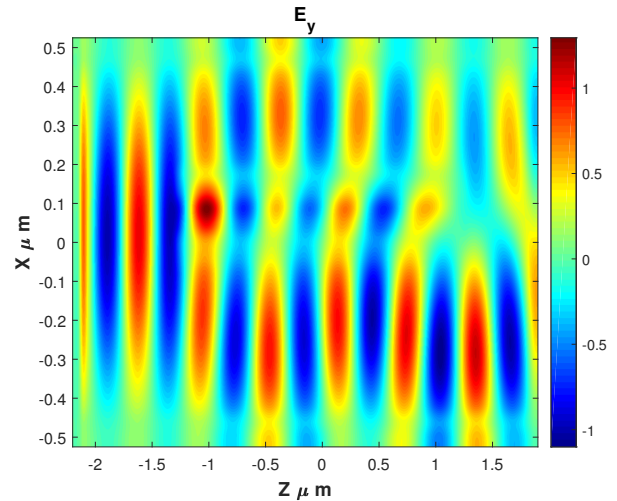
the crosstalk is also decreased to 9.2 dB with HE_{11} mode. Figure 7 shows the E_y component with respect to x and y at $z = 0.11$ μ m and wavelength of 1550 nm. It is observed that the field starts as a fundamental HE_{11} mode at the input port and ends as a first-order HE_{21} mode near the output port. The coupling effect is observed at the start of the perturbation area as a portion of the electric field is concentrated inside the SiO_2 perturbation area.

V. CONCLUSION

A mode converter based on a small material perturbation in silicon strip waveguides is proposed and its characteristics are studied. Mathematical expressions that describe the device are derived based on perturbed coupled mode theory that is used to analyze and optimize the design dimensions. An example of simple material perturbation that converts an HE_{11} to HE_{21} mode is presented, which is simply a single thin SiO_2 perturbation. Both width and position from the center of the waveguide of this SiO_2 perturbation is determined for performance optimization. Our simulation results reveal that the insertion loss of the device is 1.2 dB with a wide bandwidth around a wavelength of 1550 nm. Furthermore, this insertion loss can be improved to 0.95 dB by adding tapers to the material perturbation.

REFERENCES

[1] J. Wang, P. Chen, S. Chen, Y. Shi, and D. Dai, "Improved 8-channel silicon mode demultiplexer with grating polarizers," *Optics express*, vol. 22, no. 11, pp. 12 799–12 807, 2014. [Online]. Available: https://doi.org/10.1364/OE.22.012799

[2] H. M. H. Shalaby, "Bidirectional mode-division multiplexers with antireflection gratings," *Applied optics*, vol. 57, no. 3, pp. 476–484, 2018. [Online]. Available: https://doi.org/10.1364/AO.57.000476

[3] B. Stern, X. Zhu, C. P. Chen, L. D. Tzuang, J. Cardenas, K. Bergman, and M. Lipson, "On-chip mode-division multiplexing switch," *Optica*, vol. 2, no. 6, pp. 530–535, 2015. [Online]. Available: https://doi.org/10.1364/OPTICA.2.000530

[4] X. Guan, Y. Ding, and L. H. Frandsen, "Ultra-compact broadband higher order-mode pass filter fabricated in a silicon waveguide for multimode photonics," *Optics letters*, vol. 40, no. 16, pp. 3893–3896, 2015. [Online]. Available: https://doi.org/10.1364/OL.40.003893

[5] C. Sun, Y. Yu, G. Chen, and X. Zhang, "Integrated switchable mode exchange for reconfigurable mode-multiplexing optical networks," *Optics letters*, vol. 41, no. 14, pp. 3257–3260, 2016. [Online]. Available: https://doi.org/10.1364/OL.41.003257

[6] C. Sun, W. Wu, Y. Yu, X. Zhang, and G. T. Reed, "Integrated tunable mode filter for a mode-division multiplexing system," *Optics letters*, vol. 43, no. 15, pp. 3658–3661, 2018. [Online]. Available: https://doi.org/10.1364/OL.43.003658

[7] K. T. Ahmmed, H. P. Chan, and B. Li, "Broadband high-order mode pass filter based on mode conversion," *Optics letters*, vol. 42, no. 18, pp. 3686–3689, 2017. [Online]. Available: https://doi.org/10.1364/OL.42.003686

[8] Y.-S. Lee, K.-S. Lim, M. R. Islam, M.-H. Lai, and H. Ahmad, "Dynamic lp 01–lp 11 mode conversion by a tilted binary phase plate," *Journal of Lightwave Technology*, vol. 35, no. 16, pp. 3597–3603, 2017. [Online]. Available: https://doi.org/10.1109/JLT.2016.2599179

[9] B. E. Abu-elmaaty, M. S. Sayed, H. M. H. Shalaby, R. K. Pokharel, and S. Anand, "Silicon-on-insulator fundamental to first-order dual polarization mode converter based on si-si3n4 phase plate waveguide," in *ICTON 2018 – 20th International Conference on Transparent Optical Networks*. IEEE, 2018. [Online]. Available: https://doi.org/10.1109/ICTON.2018.8473997

[10] H. Okayama, Y. Onawa, D. Shimura, H. Yaegashi, and H. Sasaki, "Silicon wire waveguide te 0/te 1 mode conversion bragg grating with resonant cavity section," *Optics Express*, vol. 25, no. 14, pp. 16 672–16 680, 2017. [Online]. Available: https://doi.org/10.1364/OE.25.016672

[11] S.-H. Kim, R. Takei, Y. Shoji, and T. Mizumoto, "Single-trench waveguide te-tm mode converter," *Optics express*, vol. 17, no. 14, pp. 11 267–11 273, 2009. [Online]. Available: https://doi.org/10.1364/OE.17.011267

[12] A. Yariv, "Coupled-mode theory for guided-wave optics," *IEEE Journal of Quantum Electronics*, vol. 9, no. 9, pp. 919–933, 1973. [Online]. Available: https://doi.org/10.1109/JQE.1973.1077767

[13] B. E. Abu-Elmaaty, M. S. Sayed, R. K. Pokharel, and H. M. Shalaby, "General silicon-on-insulator higher-order mode converter based on substrip dielectric waveguides," *Applied optics*, vol. 58, no. 7, pp. 1763–1771, 2019. [Online]. Available: https://doi.org/10.1364/AO.58.001763

[14] O. M. Nawwar, H. M. H. Shalaby, and R. K. Pokharel, "Modeling, simulation, and fabrication of bi-directional mode-division multiplexing for silicon-on-insulator platform," *Applied optics*, vol. 57, no. 1, pp. 42–51, 2018. [Online]. Available: https://doi.org/10.1364/AO.57.000042